Hindawi
Advances in Meteorology
Volume 2019, Article ID 6357912, 16 pages
https://doi.org/10.1155/2019/6357912

*Research Article*

# Investigation into the Effects of Climatic Change on Temperature, Rainfall, and Runoff of the Doroudzan Catchment, Iran, Using the Ensemble Approach of CMIP3 Climate Models

**Abolghasem Sayadi**,[1] **Nasser Taleb Beydokhti**,[2] **Mohsen Najarchi**,[3] **and Mohammad Mahdi Najafizadeh**[4]

[1]*Department of Civil Engineering, Arak Branch, Islamic Azad University, Arak, Iran*
[2]*Faculty of Civil and Environmental Engineering, Shiraz University, Shiraz, Iran*
[3]*Department of Civil Engineering, Department of Civil Engineering, Arak Branch, Islamic Azad University, Arak, Iran*
[4]*Department of Mechanical Engineering, Arak Branch, Islamic Azad University, Arak, Iran*

Correspondence should be addressed to Nasser Taleb Beydokhti; nassertaleb@gmail.com

Received 17 August 2018; Revised 16 December 2018; Accepted 6 February 2019; Published 11 March 2019

Academic Editor: Panagiotis Nastos



This study investigated the effects of climatic changes on temperature, rainfall, and runoff in the Doroudzan catchment in the northeast of Fars province, Iran. Temperature and rainfall changes in three periods including 2011–2030, 2046–2065, and 2080–2099 were downscaled and studied using 15 Coupled Model Intercomparison Project, Phase 3 (CMIP3) climatic models, under three scenarios of greenhouse gas emissions A2, B1, and A1B, from the database of the LARS-WG model. The difference in the amount of changes in temperature and rainfall in these three periods and the observational amounts under the 15 models indicated the uncertainty of the changes values. To reduce this uncertainty and limit the results to the management and planning of water resources, ensemble approach was considered. For the preparation of the ensemble approach, the parameters from the files of the 15-model scenarios were averaged so that a climatic ensemble model could be obtained for each period. Then, the runoffs of the next three periods, under the second approach and three emission scenarios, were produced using the feedforwad neural network. The results indicated an increase in the average monthly maximum temperature and the minimum temperature in all three periods under the three scenarios. The results also showed a decrease in the rainfall in the early months of the year as well as an increase in the rainfall in the spring in most scenarios. Generally, the average annual rainfall in all these three periods under the climatic ensemble model, and three emission scenarios showed a reduction in the average annual rainfall in the three periods. The maximum amount of reduction was in 2080–2099 (101 mm) under the scenario B1. Besides, a reduction occurred in the average runoff of the catchment under three ensemble models and the emission scenario in all three periods, as compared to the average of the long-term observational values in most years.

## 1. Introduction

Climatic changes and management of the existing water resources have recently been a serious challenge worldwide. Climatic changes caused by the increase of greenhouse gasses in the earth's atmosphere result in the rise of temperature and reduction of rainfall along with drought and devastating floods in many parts of the world including Iran. Increased temperature leads to the enhanced surface water evaporation and water consumption; this, concomitant with the reduction of rainfall and surface water resources, can cause many problems for human societies. The

increased production of greenhouse gasses, especially carbon dioxide, together with overpopulation and further uses of fossil fuels due to the expansion of industries, has resulted in the rise of the earth's temperature. The wide range in the temperature increase has been predicted to be between 1.4 and 5.8 degrees in centigrade depending on the selected scenario and the AOGCM (Atmospheric-Ocean General Circulation Model) till 2100 [1]. Among the negative effects of the increased generation of greenhouse gasses, we can mention the drying up of lagoons, lakes and rivers, formation of aerosol centers, numerous environmental problems, and the adverse effects on industry, agriculture, health, and other climate-dependent systems [2]. Moreover, expansion of arid deserts and the resulting unwanted migrations and local strife are among the consequences of the climatic changes. Therefore, it is of great importance to consider climatic changes and analyze their effects on the temperature, rainfall, and runoff. To address these problems, it is necessary to investigate and analyze different possible scenarios to offer a proper solution. Consequently, planning for the proper management of surface water and underground water resources and organizing the rivers and flood warning systems require the estimation of the rivers' runoff and discharge by considering the climatic change effects. Among the valid and important measures used for the investigation of the effects of climatic changes on hydrologic and meteorological variables, one can refer to the simulation of climatic variables using AOGCM. Although these models can simplify climatic processes by simulating atmosphere-oceanic parameters for long periods of time and have a coarse special resolution, the downscaling of their output has to be done. Downscaling methods are divided into statistical and dynamic methods. Statistical methods include regression and weather generators. In order to correct the first deficiency of the general circulation models (GCMs), dynamic downscaling methods are employed. In these methods, the governing equations are solved via numerical analyses using a more scaled-down network, as compared to GCMs.

The statistical methods of downscaling are faster and less expensive than the dynamic ones [3], and the LARS-WG is a statistical model [4]. It is worth noting that a goal of the research was to study various scenarios and models of climate change on the basin. Therefore, the LARS-WG5.5 model used as the substitute contains 15 available models of the CMIP3 series, implementing under SRES emission scenarios like A1B, B1, and A2. However, while the CMIP5 series climate models are applying newer emission scenarios like RCP26, RCP45, RCP65, and RCP85, only the input data from one CMIP5 model (CANESM2) under SDSM model is available in Iran. The characteristics of the 15 AOGCM models presented in Table 1 [5–7].

Since runoff is the result of rainfall in each catchment area, it is very important to develop rainfall-runoff models. This relation is one of the most complex hydrologic processes affected by different physical and hydrologic parameters. Therefore, prediction of the catchment runoff is regarded as one of the most important issues in hydrology [8]. Due to the complex nonlinear relation between rainfall and runoff and the large number of its influential parameters, intelligent methods such as the neural network have been increasingly used in the development of rainfall-runoff models [9, 10]. Therefore, after downscaling, the GCMs output, rainfall, and temperature under different climatic models have been used as the input for the simulation of the runoffs of the future periods. Hassanzadeh et al., for instance, predicted the effect of climatic changes on river runoffs in the basin of Lake Urmia for the 2010–2100 period. To this end, they used HADCM3 (Hadley Centre Coupled Model, version 3) parameters. Besides, they calibrated and downscaled the temperature and rainfall data using LARS-WG and observational data. They also used the artificial neural network (ANN) to simulate the rainfall-runoff model. According to their results, the outputs of most models showed an increase in the temperature and a decrease in the rainfall in the next period [11]. Bahri et al. used the LARS-WG model for downscaling HADCM3 outputs under the scenario A2 for the period 2011–2030. Their results indicated a 2.7% increase in the annual rainfall, where the most reduction was in April and the most increase occurred in March. The average of minimum temperature was found to be a 3.0 to 6.1°C increase; the maximum rise of maximum temperature was estimated to be 6.1°C in May, whereas its minimum rise would be as high as 3.0°C in February [12]. Al-Safi and Sarukkalige studied the climate change effects on the hydrological response of the Richmond River catchment in New South Wales (NSW), Australia, using the Hydrologiska Byrans Vattenbalansavdelning (HBV) model. They used the monthly rainfall, temperature, runoff, evaporation, and perspiration for the long-term period of 1972–2014 to calibrate and verify the HBV model before runoff prediction. They simulated the future rainfall and runoff by a multiple ensemble model extracted from 7 GCMs through the subset of Coupled Model Intercomparison Project, Phase 3 (CMIP3), under the greenhouse gasses emission scenarios A2, A1, B, and B1. The mentioned future rainfall and runoff were used to simulate the runoffs of the three periods of the future near (2016–2043), the future middle (2044–2071), and the future far (2072–2099). In the present period, under all scenarios, a 1%–24% reduction in the annual runoff of the future periods was observed, as compared to the observational annual mean. Moreover, a reduction from 30% to 44.4% in the runoff of the future periods could be predicted, as compared to the observational values, which would help in the sustainable management and the correct use of future water resources of the Richmond catchment [13]. Kashani et al. integrated the Volterra model and the neural network (IVANN) to simulate the rainfall-runoff relation in the catchments of the northern Iran. The IVANN model was prepared using the hourly data of the runoff and rainfall with respect to 13 storms for the investigation of the short-term response of a forested catchment in the northern Iran. The catchment behavior was studied using IANN and Volterra models. The Volterra model was also used as a nonlinear model (a Second-Order Volterra (SOV) model) and solved by the Ordinary Least Squares (OLS) method. Models' performance was evaluated using five criteria: efficiency factor, the error of the mean squared error, total volume

Table 1: Characteristics of the 15 GCMs used in this study for each span: near, middle, and far.

| Model | Abbreviation | Resolution | | Duration | Longitude range (°) | Latitude range (°) | Grid number | Available emission scenario for each span | | | | | |
|---|---|---|---|---|---|---|---|---|---|---|---|---|---|
| | | | | | | | | Near and middle | | | Far | | |
| | | Longitude (°) | Latitude (°) | | | | | A1B | A2 | B1 | A1B | A2 | B1 |
| BCCR_BCM2.0 | BCM2 | 2.8125 | 2.79 | 1850–2099 | 74.53~105.47 | 25.12~41.86 | 33 | * | — | * | * | — | * |
| CCCMA_CGCM3 T47 (medres) | CGMR | 3.75 | 3.71 | 1850–2300 | 73.13~106.88 | 25.98~40.82 | 22 | * | — | — | * | — | — |
| CNRM_CM3 | CNCM3 | 2.8125 | 2.79 | 1860–2299 | 74.53~105.47 | 25.12~41.86 | 33 | * | * | — | * | * | — |
| CSIRO_Mk3.0 | CSMK3 | 1.875 | 1.8652 | 1871–2200 | 74.06~105.94 | 26.11~41.04 | 32 | * | — | * | * | — | * |
| LASG_FGOALS-g1.0 | FGOALS | 2.8125 | 2.79 | 1850–2199 | 74.53~105.47 | 25.12~41.86 | 33 | * | — | * | * | — | * |
| GFDL_CM2.0 | GFCM20 | 2.5 | 2 | 1861–2100 | 75~105 | 26~40 | 37 | * | * | * | * | * | * |
| GISS_AOM | GIAOM | 4 | 3 | 1850–2100 | 72~108 | 24~42 | 27 | * | — | * | * | — | * |
| UKMO_HadCM3 | HADCM3 | 3.75 | 2.5 | 1860–2199 | 73.13~106.88 | 26.25~41.25 | 27 | * | * | * | * | * | * |
| UKMO_HadGEM1 | HADGEM | 1.875 | 1.25 | 1860–2100 | 74.06~105.94 | 25.63~39.38 | 51 | * | * | — | — | — | — |
| INM_CM3.0 | INCM3 | 5 | 4 | 1871–2200 | 72.5~107.5 | 26~42 | 18 | * | * | * | * | * | * |
| IPSL_CM4 | IPCM4 | 3.75 | 2.535 | 1860–2230 | 73.12~103.13 | 25.35~38.03 | 29 | * | * | * | * | * | * |
| NIES_MIROC3.2 hires | MIHR | 1.125 | 1.1214 | 1900–2100 | 74.81~104.06 | 25.79~39.25 | 74 | * | — | * | * | — | * |
| MPI-M_ECHAM5-OM | MPEH5 | 1.88 | 1.87 | 1960–2200 | 74.06~105.94 | 26.11~41.04 | 32 | * | * | * | * | * | * |
| NCAR_CCSM3 | NCCCSM | 1.4063 | 1.400763 | 1890–2099 | 75.23~104.77 | 26.61~39.22 | 53 | * | * | * | * | * | * |
| NCAR_PCM | NCPCM | 2.8125 | 2.79 | 1870–2099 | 74.53~105.47 | 25.12~41.86 | 33 | * | * | — | — | — | — |

error, the relative error of the maximum error, and the time error to arrive at the peak. The results showed that IVANN could well use the semidistributed and distributed models for simulating the rainfall trend. Compared to the integrated models, the distributed SOV model has a lower precision for the rainfall trend simulation [14]. Li et al. also explored the impacts of climatic changes on the water resources of the Grand River catchment in Ontario, Canada, by developing the two-phase model of Providing Regional Climates for Impacts Studies (PRECIS) and Hydrological Inference Model (HIM). They simulated future rainfall and runoff (2071–2100) under the two emission scenarios A2 and B2 using the PRECIS model. Their results showed that although the annual rainfall of the future period did not considerably change, as compared to the observational values, a change occurred in the trend of the annual rainfall. Rainfall was found to increase in winter and decrease in summer. Therefore, for the proper conformity to the new conditions, some changes were required for planning and managing the water resources [15]. Mislan et al. also employed Back-propagation Neural Network (BPNN) for the monthly prediction of the rainfall in Tenggarong Station, Indonesia. They used the architectures of [2-50-10-1, epoch 500] and [2-50-20-1, with the epochs 1000 and 1500]. According to their results, [2-50-20-1, with the epochs 1000] had the best performance in the prediction of the monthly rainfall based on the mean squared error (MSE) [16]. Farajzadeh et al. also predicted the runoff of the Urmia Lake Basin using the neural network. Climatic changes, construction of causeway over the lake, establishment of several dams, and overuse of water resources for agricultural purposes led to the sharp drop of the lake level and creation of acres of salt marsh. Therefore, due to the importance of predicting the basin runoff, they used the feedforward neural network and time series analysis [17]. Further, Asadi et al. used a hybrid intelligent model to predict runoff. Their suggested model was a combination of data preprocessing, genetic algorithm, and Levenberg Marquard (LM) learning algorithm for learning the feedforward neural networks. In fact, by using the genetic algorithm, the original weights of the neural network were developed for regulation with the LM algorithm. Besides, they used data preprocessing approaches such as data transfer, selection of input variables, and data clustering to improve the model precision. They also examined the model capability for the prediction of runoff in the Aghchai catchment. According to them, their model could predict runoff more exactly in comparison to ANN and ANFIS models [18]. Solaimani compared three different learning algorithms of gradient descent (GDX), conjugate gradient (CG), and LM for the rainfall-runoff prediction based on the artificial neural network. Monthly hydrometric data and weather information were used to develop the artificial neural network. By combining the computational efficiency with the input parameters characterizing meteorological information, ANN prediction performance could be improved. Based on their results, GDX learning algorithm was found to have the highest precision and convergence speed, but the LM algorithm had the lowest speed [19–21].

## 2. Materials and Methods

*2.1. Simulation of Climatic Changes.* The Doroudzan catchment is situated in the northeast of Fars province, Iran (Figure 1).

The dam constructed on this catchment satisfies a major part of water requirements for industry, agriculture and fresh water applications in downstream cities including Shiraz. First, the climatic change effects on the rainfall, temperature and sunny hours of the catchment were examined using LARS-WG. Here, 15 climatic models of CMIP3 series existing in the LARS-WG model database [22] under the greenhouse gas emission scenarios B1, A2, and A1B were utilized to provide the data related to three future periods including 2011–2030, 2046–2065, and 2080–2099 for all the stations of the Doroudzan catchment.

15 climatic models from the LARS-WG model database under the three greenhouse gas emission scenarios B1, A2, and A1B for the three future periods of 2011–2030, 2046–2065, and 2080–2099 were implemented on six meteorology stations according to Tables 2 and 3. In other words, 15 models were used for each station, with a maximum of three emission scenarios for each model in the mentioned three periods. In order to verify the LARS-WG results, the data quality was first controlled by the model itself; then the statistics of the simulated data, such as average, standard deviation, and length of wet and dry periods (in terms of rainfall), were calculated. In the next stage, the model simulated and produced the meteorological data (e.g., temperature, rainfall, and sunny hours) for the same time period, generating the corresponding statistics of the observational data. In order to verify and ensure model precision, $t$ (Table 4), $F$ (Table 5), and K-S (Tables 6 and 7) tests were performed; then, the average, standard deviation, and goodness of fit of the two data series were compared. By ensuring model precision for any meteorology station, the corresponding data related to rainfall, temperature, and sunny hours in the mentioned three future periods under 15 climatic models and three greenhouse gas emission scenarios were simulated. As an example, here, the verification results of the LARS-WG model of the Doroudzan station have been summarized. The $t$-test was used to compare the averages of the two data series. If the $P$-Value takes greater than 0.05, then no significant difference would be observed between the averages of them. The assessment value specifies by the amount of $P$-Value. Approaching it to 1 means to the higher the assessment value. In any case, if $P$-Values take more than 0.05 means to the result, it is acceptable (O.K), and the averages of the monthly observational and simulated data by the model are close enough [23]. If $P$-Value takes less than 0.05, means to the assessment is poor, and the result is not acceptable (N.G).

As can be clearly seen from Table 6, the model could well simulate the length of wet and dry periods for different seasons; hence, the probabilistic distributions of the two series of observational and simulated data for the basic period were found to be quite similar.

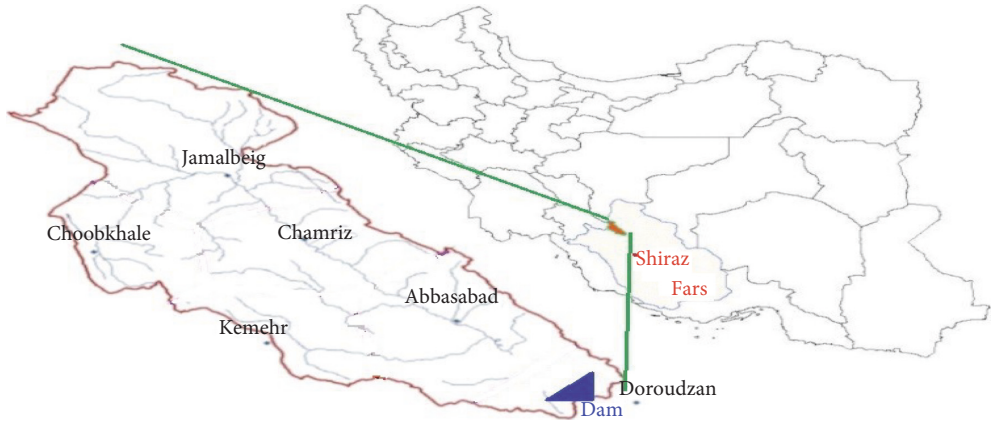


Figure 1: Position of the stations under study.

Table 2: Features of the stations under study.

| Station | River | UTMY (m) | UTMX (m) | Height (m) | Weight (%) |
|---|---|---|---|---|---|
| Doroudzan | Kor | 3342946 | 638943 | 1652 | 19.00 |
| Choobkhale | Choobkhale | 3379456 | 585762 | 2040 | 8.59 |
| Kemehr | Kor | 3368805 | 584103 | 2377 | 9.18 |
| AbbasAbad | Kor | 3354465 | 620649 | 1713 | 24.63 |
| Jamalbeig | Shirin | 3386581 | 591422 | 2020 | 19.00 |
| Chamriz | Kor | 3370902 | 605703 | 1850 | 19.59 |

UTMX and UTMY refer to the position of each station in the Universal Transverse Mercator geographical coordinate system (UTM-zone 39N).

Table 3: The annual and monthly average of the precipitation of the Doroudzan catchment stations (mm).

| Station | Jan | Feb | Mar | Apr | May | Jun | Jul | Aug | Sep | Oct | Nov | Dec | Annual |
|---|---|---|---|---|---|---|---|---|---|---|---|---|---|
| Kemehr | 193.88 | 175.33 | 191.58 | 110.08 | 17.88 | 0.50 | 1.63 | 0.83 | 1.96 | 12.63 | 132.92 | 168.33 | 1007.54 |
| Jamalbeig | 107.11 | 88.81 | 93.04 | 57.71 | 18.28 | 0.71 | 0.59 | 0.57 | 0.05 | 6.36 | 41.00 | 112.35 | 526.57 |
| Doroudzan | 130.94 | 107.27 | 82.29 | 40.09 | 5.76 | 0.42 | 1.11 | 0.41 | 0.04 | 3.88 | 34.73 | 109.81 | 516.74 |
| Choubkhale | 161.08 | 152.76 | 153.88 | 103.00 | 29.38 | 1.80 | 1.83 | 1.20 | 0.50 | 10.86 | 70.24 | 172.75 | 859.29 |
| Chamriz | 97.04 | 66.75 | 73.00 | 35.92 | 8.13 | 0.00 | 0.83 | 0.21 | 0.00 | 3.04 | 59.46 | 75.54 | 419.92 |
| Abbasabad | 96.97 | 76.34 | 69.19 | 35.46 | 6.77 | 0.08 | 0.08 | 0.85 | 0.00 | 3.04 | 61.54 | 74.65 | 424.98 |
| Average | 119.8 | 98.35 | 95.46 | 53.3 | 12 | 0.4 | 0.8 | 0.6 | 0.2 | 5.38 | 59.43 | 105.7 | 551.47 |

Table 4: Results of the *t*-test, comparison of the average monthly observational and LARS-WG simulated rainfalls of the Doroudzan station.

| Item/Month | J | F | M | A | M | J | J | A | S | O | N | D |
|---|---|---|---|---|---|---|---|---|---|---|---|---|
| Observational rainfall | 112 | 94.72 | 75.1 | 39.95 | 6.25 | 0.32 | 0.74 | 0.26 | 0.09 | 5.45 | 46.4 | 87.06 |
| Simulated rainfall | 128 | 97.66 | 85.5 | 38.35 | 6.52 | 0.31 | 1.6 | 0.24 | 0.38 | 6.29 | 39.8 | 84.17 |
| *t*-test | −0.9 | −0.183 | −0.8 | 0.198 | −0.1 | 0.043 | −0.98 | 0.098 | −1.61 | −0.378 | 0.499 | 0.17 |
| *P*-value | 0.37 | 0.855 | 0.43 | 0.844 | 0.921 | 0.966 | 0.33 | 0.922 | 0.113 | 0.707 | 0.62 | 0.866 |
| Assessment | Good | Prefect | Good | Prefect | Prefect | Prefect | Good | Prefect | Good | Very good | Very good | Prefect |
| Result | O.K | O.K | O.K | O.K | O.K | O.K | O.K | O.K | O.K | O.K | O.K | O.K |

Table 5: Results of the *F*-test, standard deviation comparison of observational and simulated data by the model of the Doroudzan station.

| Item/month | J | F | M | A | M | J | J | A | S | O | N | D |
|---|---|---|---|---|---|---|---|---|---|---|---|---|
| sd_obs | 69.28 | 69.31 | 51.91 | 35.02 | 10.96 | 0.88 | 2.63 | 1.13 | 0.36 | 9.19 | 51.72 | 81.80 |
| sd_gen | 76.48 | 61.91 | 53.82 | 31.34 | 11.28 | 1.00 | 4.07 | 0.89 | 0.93 | 8.94 | 55.12 | 58.97 |
| *F*-test | 1.22 | 1.25 | 1.08 | 1.25 | 1.06 | 1.29 | 2.39 | 1.64 | 6.62 | 1.06 | 1.14 | 1.92 |
| *P*-value | 0.60 | 0.51 | 0.86 | 0.52 | 0.89 | 0.49 | 0.02 | 0.16 | 0.00 | 0.86 | 0.74 | 0.06 |
| Assessment | Very good | Good | Prefect | Good | Prefect | Good | Poor | Good | Poor | Prefect | Very good | Good |
| Result | O.K | O.K | O.K | O.K | O.K | O.K | N.G | O.K | N.G | O.K | O.K | O.K |

sd_obs and sd_gen are standard divisions of observational and produced data by the model, respectively.

Table 6: Results of the K-S test: goodness of fit comparison between two time series of observational rainfall data and the simulation of the Doroudzan station.

| Season | Wet/dry | $N$ | K-S | $P$ value | Assessment |
|---|---|---|---|---|---|
| DJF | Wet | 12 | 0.34 | 0.1097 | Good fit |
| DJF | Dry | 12 | 0.052 | 1 | Perfect fit |
| MAM | Wet | 12 | 0.081 | 1 | Perfect fit |
| MAM | Dry | 12 | 0.188 | 0.7665 | Very good fit |
| JJA | Wet | 12 | 0 | 1 | Perfect fit |
| JJA | Dry | 12 | 0.174 | 0.8416 | Very good fit |
| SON | Wet | 12 | 0.287 | 0.2522 | Good fit |
| SON | dry | 12 | 0.171 | 0.8563 | Very good fit |

Table 7: Results of the K-S test for the daily rainfall.

| Month | $N$ | K-S | $P$ value | Assessment |
|---|---|---|---|---|
| J | 12 | 0.037 | 1 | Perfect fit |
| F | 12 | 0.055 | 1 | Perfect fit |
| M | 12 | 0.059 | 1 | Perfect fit |
| A | 12 | 0.112 | 0.9975 | Perfect fit |
| M | 12 | 0.139 | 0.9685 | Perfect fit |
| J | 12 | 0.174 | 0.8416 | Very good fit |
| J | 12 | 0.348 | 0.0955 | Good fit |
| A | 12 | 0.609 | 0.0002 | Proof fit |
| S | 12 | 0.435 | 0.0173 | Proof fit |
| O | 12 | 0.237 | 0.4809 | Good fit |
| N | 12 | 0.044 | 1 | Perfect fit |
| D | 12 | 0.053 | 1 | Perfect fit |

Note that $t$, $F$, and K-S tests were conducted on rainfall, $T_{\min}$ (minimum daily temperature), and Tmax (maximum daily temperature) of all stations. After ensuring model precision, it generated time series of them in three periods of future near, middle, and far different stations under 15 CMIP3 models and three emission scenarios.

After model verification, data related to rainfall, temperature, and sunny hours in three future periods and under three emission scenarios for 15 climate models in all stations were generated and the results were averaged. Then, they were compared with the observational data. By comparing the results of different models under the main three emission scenarios, it could be observed that there were some differences in the results, which could be due to the uncertainty of emission scenarios, different dimensions of the cells in different models, boundary conditions, and the solution method of the governing equations by each climatic model and the existing errors in the simulation and production of the model data. Therefore, there was a wide range of climate models for the future predictions. In order to limit the predictions to a few models that could be used for the investigation of climatic change effects, three approaches were considered: extreme (min/max), ensemble approach, and validation approach. The min/max approach was the best way for planning in a wide range of considerations; it involves plans for both maximum and minimum changes. Ensemble approach suggests that it is better to plan for the average changes of all models. This approach uses a unique average or mean for all (or most) of the models for reducing uncertainty. The individual model of validation approach suggests that the chronologically appropriate models should be used for planning in the meteorological observations. These observations compare a chronological (over-thirty-year) global dataset (e.g., National Center Environment Prediction (NCEP)) with all models to determine to which models the dataset best conforms. After that, only the four or five models having the most conformity are used. In the present study, the Ensenble approach was employed [22, 24].

In order to develop the ensemble approach, the following steps were taken. First, values of columns 2 to 7 of the scenario file of each of the 15 models were extracted and averaged. The average was then introduced as a climatic scenario file called ensemble into the LARS-WG model, and the future data scenario for three future periods under the said emission scenario was created. Therefore, an ensemble climatic model was added to the previous 15 models. In what follows, figures of Tmin and Tmax and daily rainfall changes using 15 CMIP3 models and ensemble approach under three emission scenarios for the three future periods are represented (Figures 2 to 4).

It is clear from row 1 of Figure 2 that the maximum increases of Tmin for the future near period under the scenarios A1B, A2, and B1 could be expected to be in July with the temperature of 3.96°C under the HADGEM model, 3.78°C under HADGEM and HADCM3 models, and 3.86°C under the IPCM4 model, respectively.

Moreover, the maximum decrease of Tmin was in January under the HADCM3 model with the amount of 0.43, 0.25, and 0.54°C. Except for some models in January, a rise was observed for all models in the other months of the year. Row 2 of Figure 2 shows that the maximum increase of the Tmin for the future middle period under scenarios A1B, A2, and B1 were in May under the GFCM2 (3.41°C), and in September under GFCM2 (3.1°C), and MIHR (2.96°C) models, respectively. Besides, the minimum rise was in January under CSMK3 (2°C), NCPCM (1.8°C), and BCM2 (−0.03°C) models, respectively. Clearly, all of the models predicted a rise in the future middle time under all three scenarios. Clearly, in the third row, the maximum increase of the Tmin in the future far period expected would be in May under the MIHR model (6.0°C). Obviously, it predicted to rise with 100% certainty under all scenarios.

Row 1 of Figure 3 shows that the maximum increase of the Tmax for the future near period under the scenarios A1B, A2, and B1 was expected in July with 1.8°C under the CGMR, at 1.7°C under the NCCCSM, and at 1.17°C under NCCCSM and INCM3 models, respectively. Moreover, the maximum decrease of Tmax was estimated to be in January under the HADCM3 with the rise of 0.9°C and February under NCPCM, FGOALS, and CSMK3 models, 0.8°C. Except for some models in January and February, a rise was observed for all the models in the other months of the year. It is clear from second-row figures that the highest increase in the $T_{\max}$ (future middle period) was in July under the climatic model of MIHR under the scenario A1B, whereas the least increase was in January under the CSMK3 model under the scenario

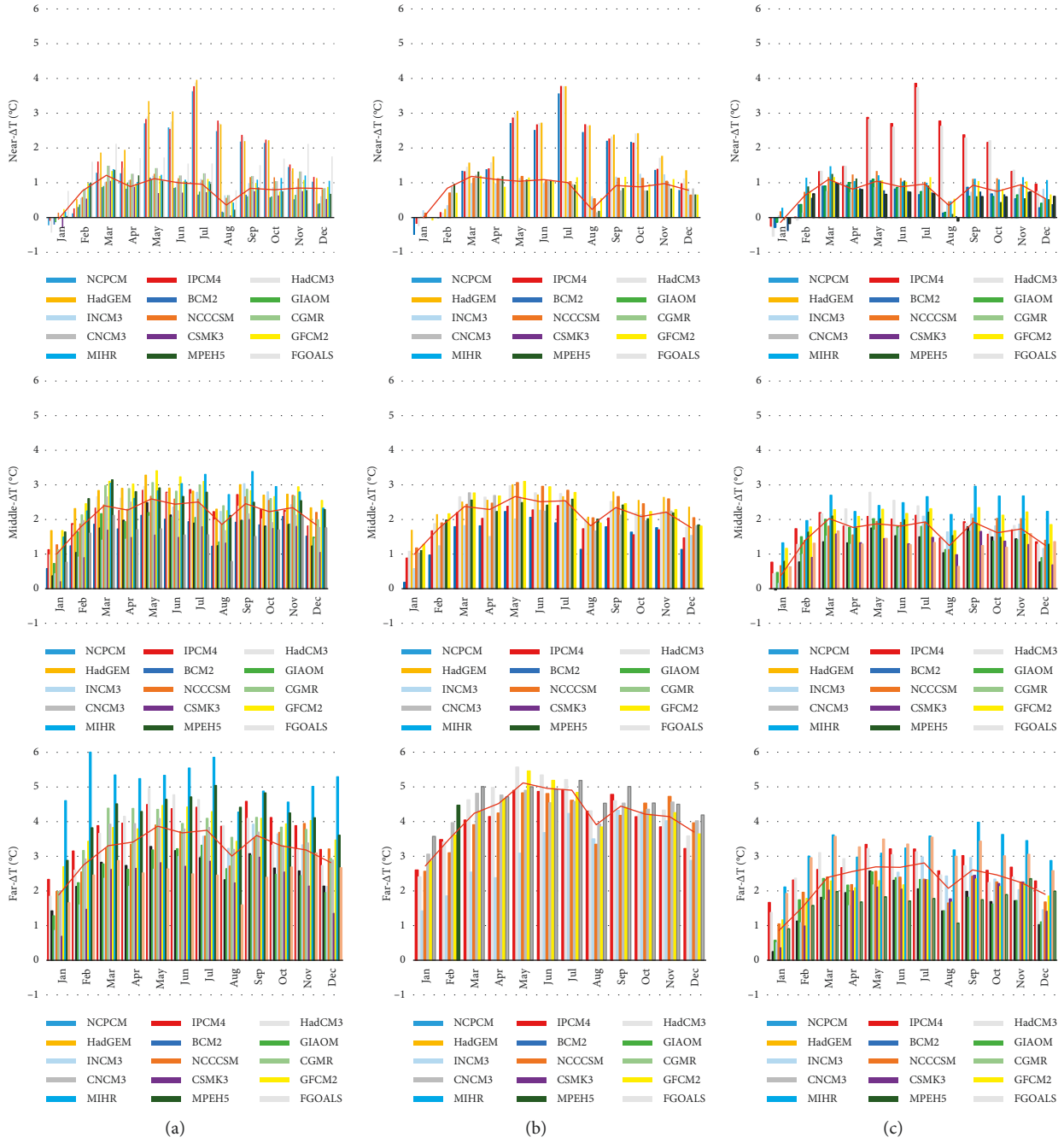


Figure 2: Tmin changes under different GCMs and ensemble approach versus observational values for the three future period under scenarios (a) A1B, (b) A2, and (c) B1.

A1B (0.49°C). Also, for each climatic parameter such as rainfall and temperature, a total of 35 models and scenarios were investigated monthly, and 420 cases were considered for 12 months. There were only 26 cases of temperature drop. In other words, in 94% of the cases, the Tmax would be increased. Further, the third-row figures show that the most and the least amounts of increase in the future far period expected would be 6.31°C and −0.095°C, respectively. Also, the area has a desert climate. Consequently, the large fluctuation of the monthly Tmax is due to climatic conditions, especially the type of weather situation.

According to row 1 of Figure 4, in the future near period, a decrease could occur in the amount of rainfall in most models in January and February, while it might increase in March, April, May, October, November, and December, indicating a change in the annual rainfall pattern. In order to tackle this problem, environmental planning and management of water resources will be required. Figures in the second row show that the trend of changes in the annual rainfall in the future middle period is similar to that of the near one. The highest increase in the monthly rainfall was observed under the MPEH5 model in the scenario B1

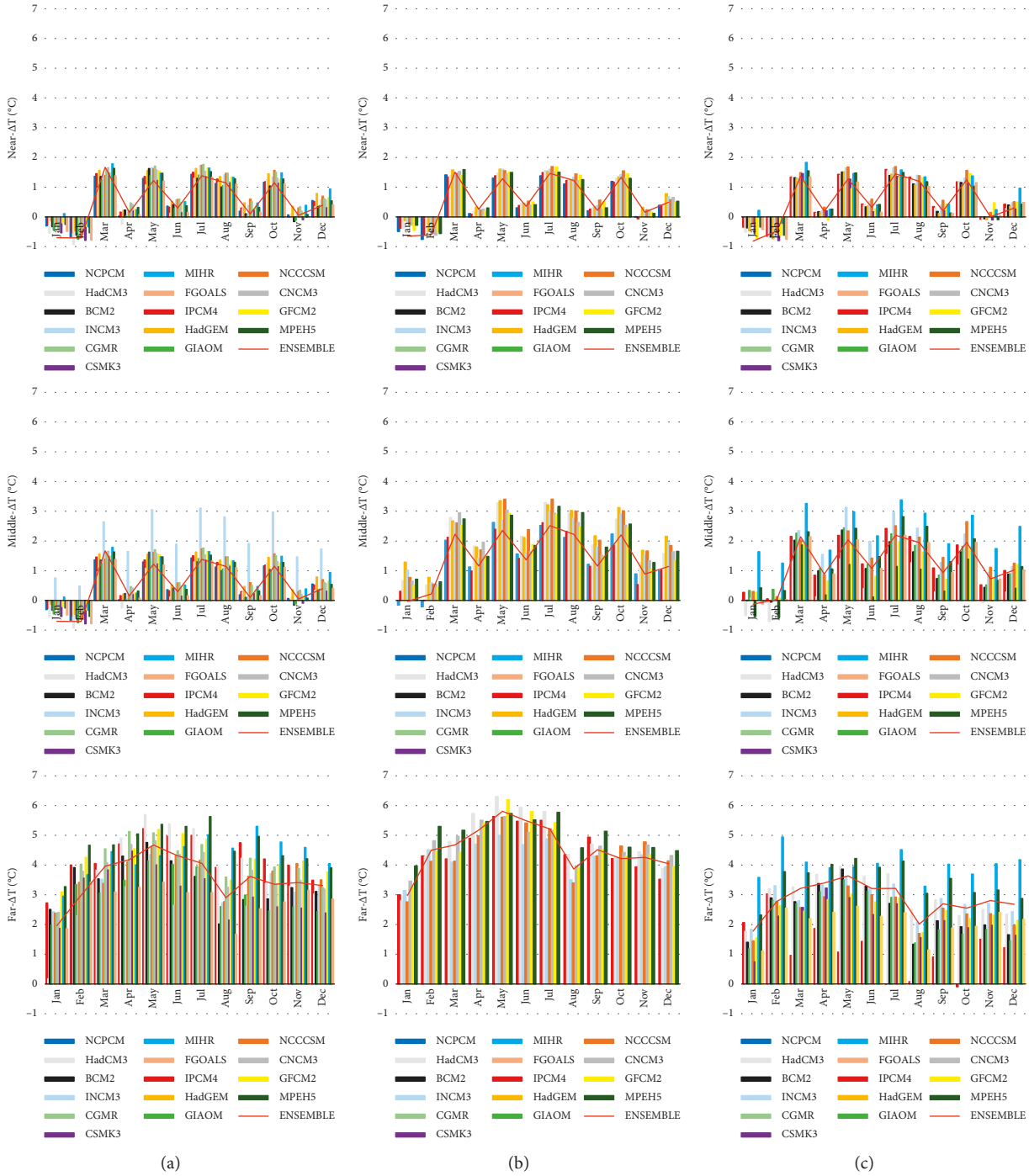


FIGURE 3: Tmax changes under different GCMs and ensemble approach versus the observational values for the three future periods under scenarios (a) A1B, (b) A2, and (c) B1.

(53 mm), and the least decrease in the monthly rainfall was under the GFCM2 model in the scenario A2 (44 mm) in February. Patterns of changes in the annual precipitation in the future far period (row 3) were similar to those in the two other periods. In this period, the maximum increase of the annual rainfall was predicted to be 79.2 mm in December under IPCM4 model in the scenarios A1B and B1. Besides, the maximum decrease was expected to be 57.2 mm in February under MPEH5 and the scenario A2.

In the above figures, $\Delta T$ and $\Delta P$, respectively, are average of the monthly changes of daily temperature (minimum and maximum) in centigrade and monthly precipitation (rainfall) in millimeter versus the observational values. In what follows, the range of changes of the monthly rainfall and temperature in the three future periods under all available models and the three emission scenarios (35 states) and their probabilities (i.e., increases) versus the observational values are given (Figures 5–10).


FIGURE 4: Monthly rainfall changes under different GCMS, ensemble approach versus observational values in the tree future period for the three future period under scenarios (a) A1B, (b) A2, and (c) B1.

Due to the fact that precipitation decreases in the early months of the future years and increases in the last months of the future years, as compared to the observational values, the annual future precipitation and the average of observational values have been compared and diagramed here.

Based on the results, a reduction occurred in precipitation in most years of each period versus the average annual observational values of the basic period. Furthermore, based on Figure 11, the average of the annual rainfall in each period decreased as compared to the average of the annual observational precipitation (AAOP).

Figure 12 shows that the average annual precipitation changes in all three future periods, as compared to the observational value, which would decrease. Based on this figure, the maximum reduction could be in the far future period under the scenario B1, and the minimum one would be in the near future period under the scenario A2, which could be as great as 0 mm.

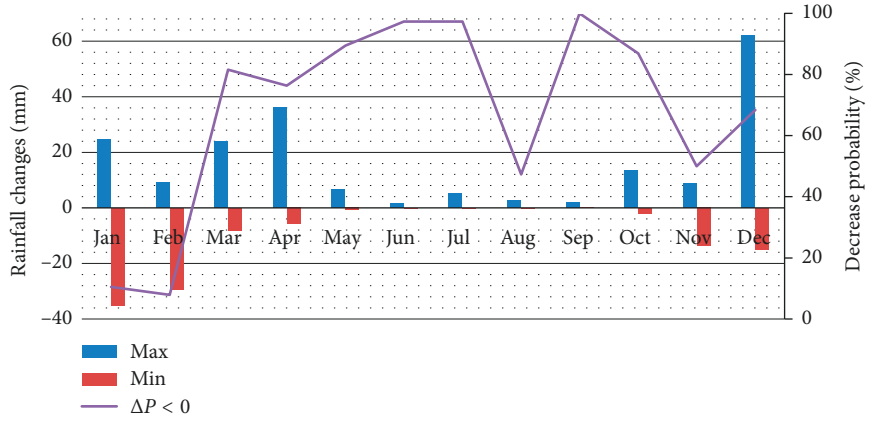


Figure 5: Range of changes in the monthly rainfall in the future near period under all the models and the three emission scenarios and their probabilities.

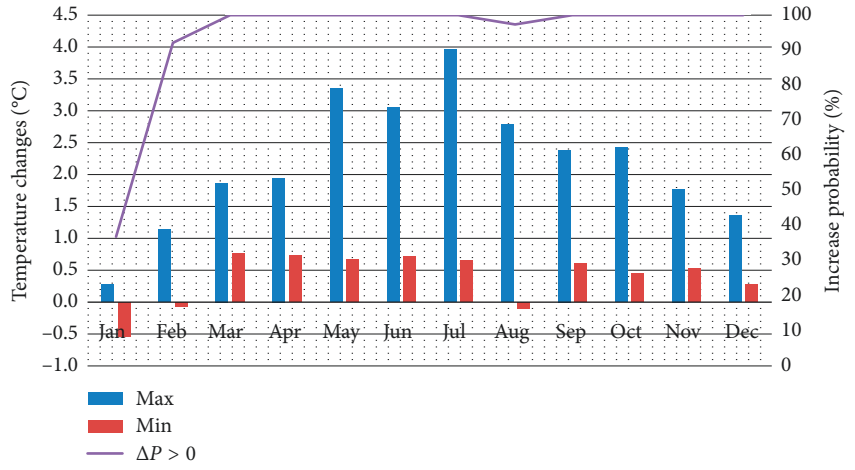


Figure 6: Range of changes in the monthly average of minimum daily temperature in the future near period under all the models and three emission scenarios and their probabilities.

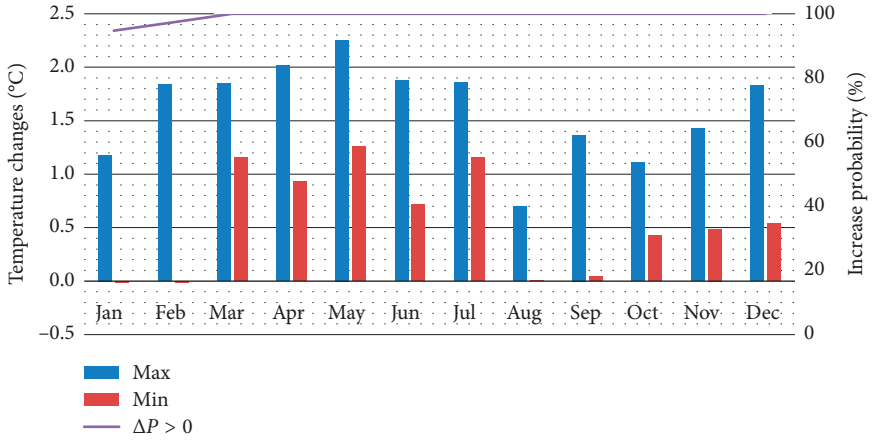


Figure 7: Range of changes in the monthly average of the maximum daily temperature in the future near period under all the models and three emission scenarios and their probabilities.

*2.2. Application of Neural Network in the Determination of the Future Discharge of the Doroudzan Dam.* In order to determine the input discharge (runoff) entering into the Doroudzan dam in the three future periods, it was required to model the rainfall-runoff relation. To this end, the neural network has been employed. After measuring rainfall and

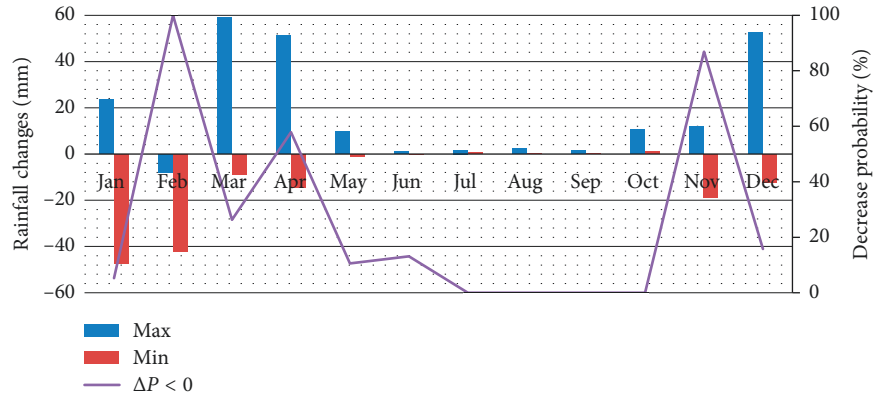


Figure 8: Range of changes in the monthly rainfall in the future middle period under all models and three emission scenarios and their probabilities.

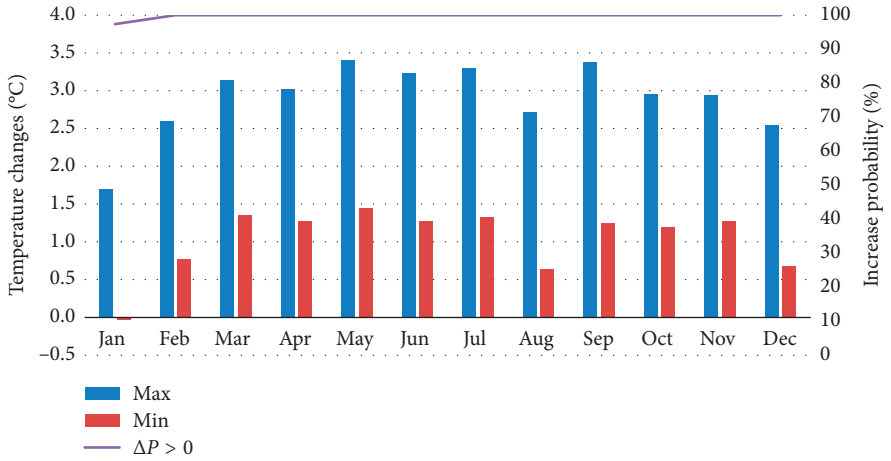


Figure 9: Range of changes in the monthly average of the minimum daily temperature in the future middle period under all models and three emission scenarios and their probabilities.

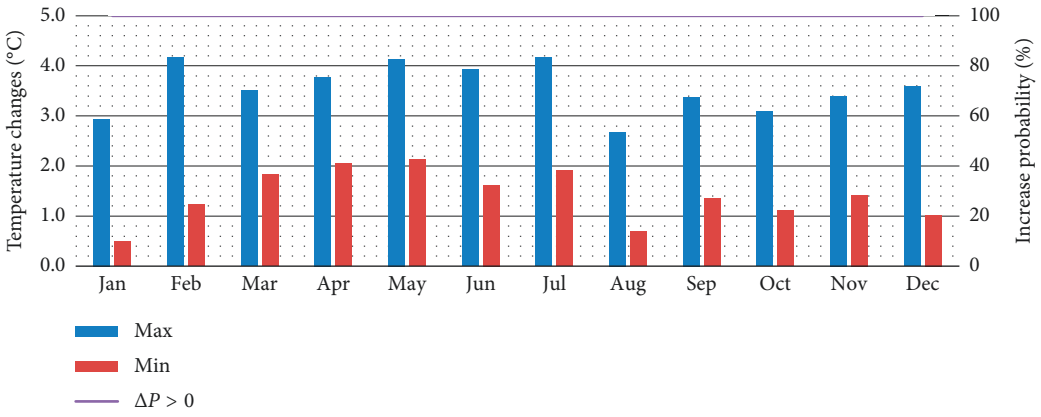


Figure 10: Range of changes in the monthly average of the maximum daily temperature in the future middle period under all the models and three emission scenarios and their probabilities.

temperature in the future periods based on different models and scenarios, due to their wide range of variations under all the models, the results of the ensemble model (rainfall and temperature) were used for simulating the future runoff. First, by considering different combinations of rainfall, temperature, and runoff time series of the last few days as the

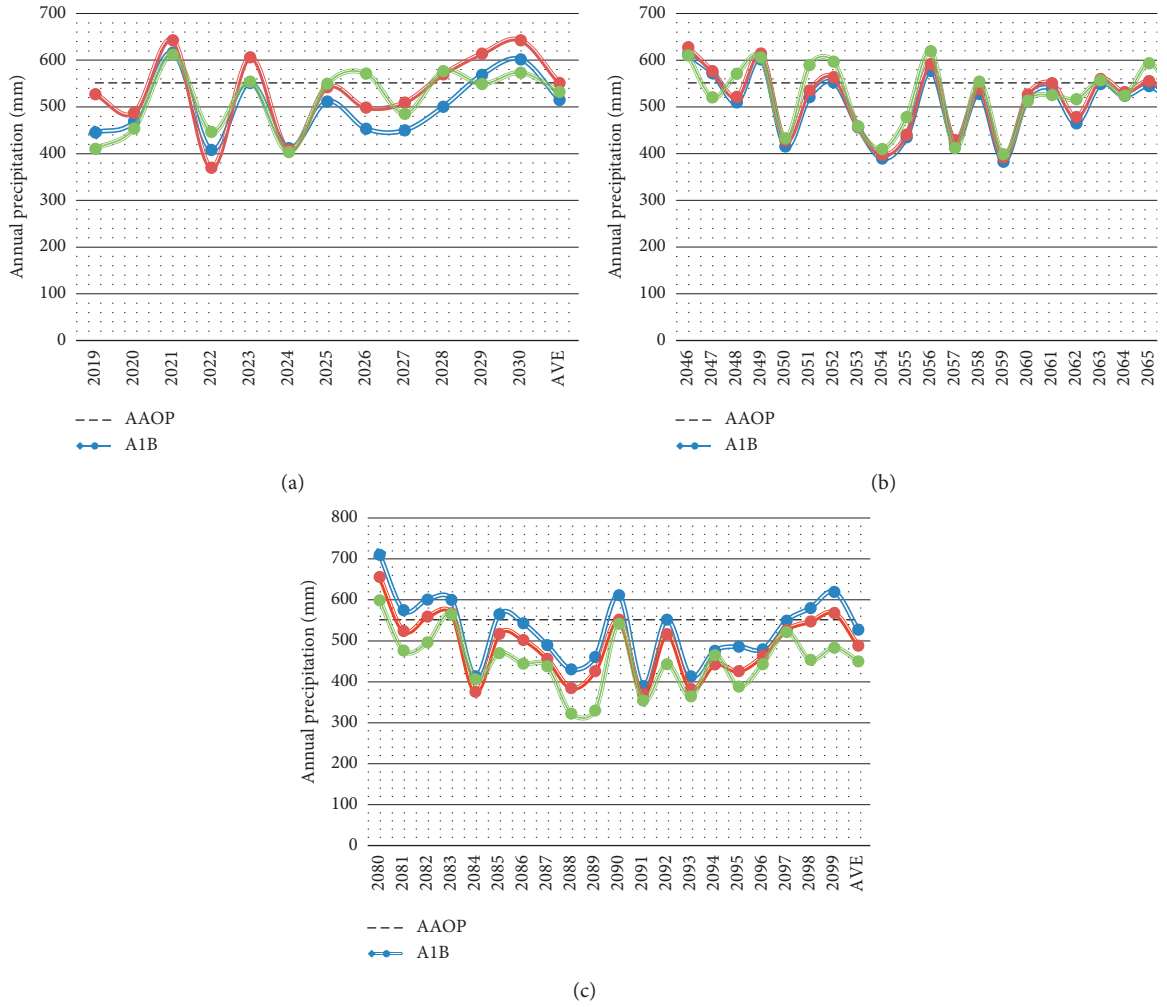


Figure 11: Changes in the averages of the annual rainfall in the future periods under ensemble model and three emission scenarios versus the observational values: (a) near future, (b) middle future, and (c) far future.

input and runoff as the output, the best architecture and type of the neural network with the least errors and the highest correlation coefficient were defined; then the future-period runoff entering the catchment was determined.

To model the rainfall-runoff relation of the catchment using the artificial neural network, different neural networks, learning algorithms, numbers of hidden layers, available neurons in the hidden layers, activation function, etc., were selected and tested. Among them, the best neural network and architecture were chosen. Note that first, the daily and then the monthly data were utilized. Due to the fact that the daily rainfall data, as one of the most important input data in the rainfall-runoff model, involve many zeros, it involves more errors than the rainfall-runoff model using the monthly data. In other words, it is difficult and less likely to arrive at a proper neural network model by using daily data including the rainfall data. However, in rainy areas, the learning of the rainfall-runoff model is perhaps easier due to the high number of the daily rainfall nonzero data. In what follows, different kinds of neural networks are studied and their performances are summarized (Table 8).

In the above table, generalized feedforward (GFF) neural network was chosen due to its performance and compared to some other neural networks such as multilayer perceptron (MLP) and radial basis function (RBF). By comparing the LM and Conjugate Gradient (CG) [25, 26], it was found that CG had a better performance in the neural network learning. GFF neural network is an artificial neural network in which the connection of its constituent units does not form a cycle. In fact, this network is different from the recurrent neural network. In addition, the feedforward neural network is the first and the simplest kind of the artificial neural network. In this network, the information moves only in a forward direction. In fact, it moves from the input nodes (neurons) through the innate layers (if any) to the output nodes [25, 26]. Activation functions, namely, TANGENT HYPERBOLIC (TANH), LINEAR TANGENT HYPERBOLIC (LTANH), and LINEAR SIGMOID (LSIG), were also tested and used.

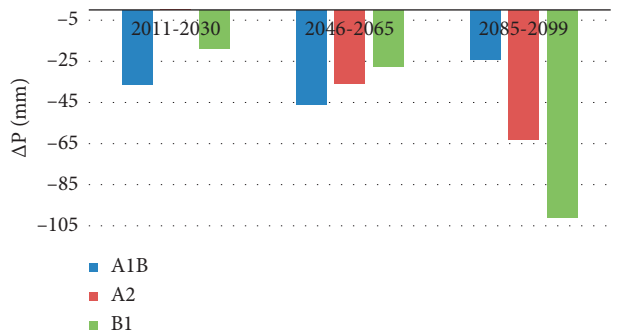


Figure 12: Comparison of the average annual observational value and the three future periods under three emission scenarios.

Table 8: Performances of different neural networks concerning the monthly rainfall-runoff model for the Doroudzan catchment.

| Ann type | Input | Output | Learning algorithm | Network architecture | Transfer function | | Data percentage | | | RMSE | | | $r$ |
|---|---|---|---|---|---|---|---|---|---|---|---|---|---|
| | | | | | First | Second | Learning | Validation | Test | Learning | Validation | Test | |
| GFF | Tave,P,E | Q | CG | 3-4-4-1 | TANH | LTANH | 65 | 15 | 25 | 0.15 | 0.32 | 19.13 | 0.840 |
| | Tave,P,E | Q | CG | 3-15-8-1 | TANH | LTANH | 65 | 15 | 25 | 0.15 | 0.23 | 38.66 | 0.719 |
| | Tave,P,E | Q | CG | 3-4-4-1 | TANH | LTANH | 65 | 15 | 25 | 0.12 | 0.65 | 35.69 | 0.586 |
| | Tave,P,E | Q | CG | 3-4-4-1 | TANH | LTANH | 80 | 10 | 10 | 0.10 | 1.18 | 34.99 | 0.600 |
| | Tave,P,E | Q | CG | 3-4-4-1 | TANH | LTANH | 70 | 10 | 20 | 0.19 | 0.20 | 44.98 | 0.597 |
| | P,E | Q | CG | 2-4-4-1 | TANH | LTANH | 70 | 10 | 20 | 0.15 | 0.28 | 27.18 | 0.670 |
| | P,Tave | Q | CG | 2-4-4-1 | TANH | LTANH | 70 | 10 | 20 | 0.15 | 0.28 | 34.18 | 0.61 |
| | P-3,P-2,P-1,P | Q | CG | 4-4-4-1 | TANH | LTANH | 75 | 10 | 15 | 0.0080785 | 0.02670124 | 17.50 | 0.726 |
| | P-3,P-2,P-1,P | Q | CG | 4-14-10-1 | TANH | LTANH | 75 | 10 | 15 | 0.00249497 | 0.00467218 | 46.12 | 0.238 |
| | P-3,P-2,P-1,P | Q | CG | 4-4-4-1 | TANH | LTANH | 75 | 10 | 15 | 0.00268782 | 0.00762632 | 20.11 | 0.911 |
| | P-2,P-1,P | Q | CG | 3-4-4-1 | TANH | LTANH | 75 | 10 | 15 | 0.0176 | 0.0232 | 54.23 | 0.530 |
| | P-1,P | Q | CG | 2-4-4-1 | TANH | LTANH | 75 | 10 | 15 | 0.0324 | 0.02670124 | 17.5 | 0.48 |

$$f(x) = \mathrm{TANH}(x) = \frac{e^{x} - e^{-x}}{e^{x} + e^{-x}},$$

$$f(x) = \mathrm{LTANH}(x) = \begin{cases} -1, & \text{if } x_i^{\mathrm{lin}} < -1, \\ 1, & \text{if } x_i^{\mathrm{lin}} > 1, \\ x_i^{\mathrm{lin}}, & \text{else}, \end{cases} \tag{1}$$

$$f(x) = \mathrm{LSIG}(x) = \begin{cases} 0, & \text{if } x_i^{\mathrm{lin}} < 0, \\ 1, & \text{if } x_i^{\mathrm{lin}} > 1, \\ x_i^{\mathrm{lin}}, & \text{else}, \end{cases}$$

where $x_i^{\mathrm{lin}} = \beta x_i$ is the scaled and offset activity inherited from the Linear Axon. The LinearSigmoidAxon substitutes the intermediate portion of the sigmoid by a line of slope $\beta$, making it a piecewise linear approximation of the sigmoid. Performance of each neural network was assessed using the Root Mean Square Error (RMSE) and the Pearson Correlation Coefficient ($r$).

$$\mathrm{RMSE} = \sqrt{\frac{\sum_I^n (O_i - S_i)}{n}},$$

$$r = \frac{\sum_i^n (O_i - \overline{O}) \sum_i^n (S_i - \overline{S})}{\sqrt{\sum_i^n (O_i - \overline{O})^2 \sum_i^n (S_i - \overline{S})^2}}, \tag{2}$$

where $O$ is the observational data, $S$ is the simulated data, $\overline{O}$ and $\overline{S}$ are their averages, and $n$ is the total number of the data.

Perhaps, since normalized values were used for learning and validation, RMSE values were smaller than 1; however, the data in the test step are not normalized; so RMSE values did not need to be lower than 1. Performance of the selected neural network in the test step is shown in Figure 13, indicating the selected network's precision.

Table 9 shows the performance of the selected neural network at the test step. After the determination of the proper neural network, the runoff data for the future periods were generated. The output of the ensemble model under the three emission scenarios (monthly rainfall) was used as the input of the neural network. Figure 14 shows runoffs in the

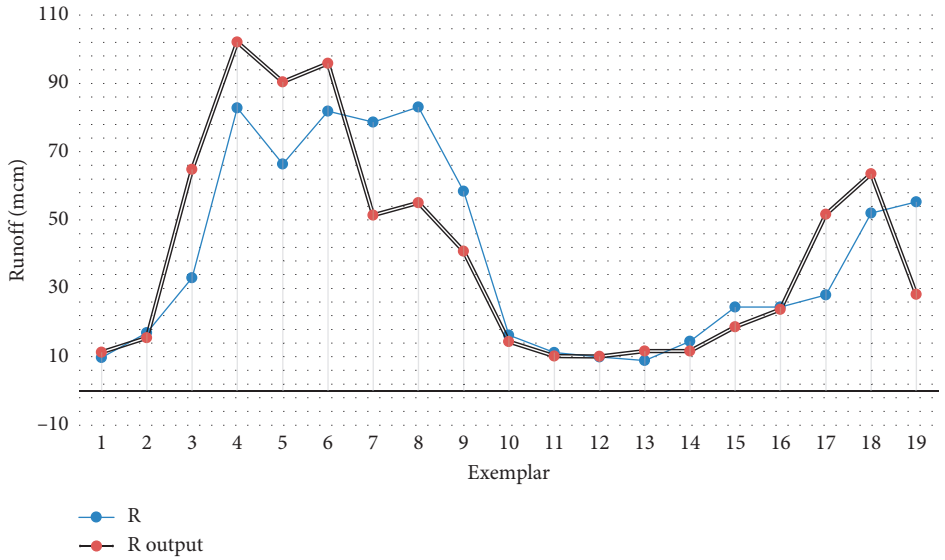


Figure 13: Observational runoff—monthly simulation of the Doroudzan dam in the neural network test step. $R$ = the observational runoff; $R$ = output the runoff simulated by the neural network.

Table 9: Performance of the neural network for the monthly rainfall-runoff in the Doroudzan dam in the test step.

| Performance | Test step |
|---|---|
| MSE | 404.3462945 |
| RMSE | 20.10836379 |
| MAE | 16.850975 |
| $r$ | 0.911308447 |

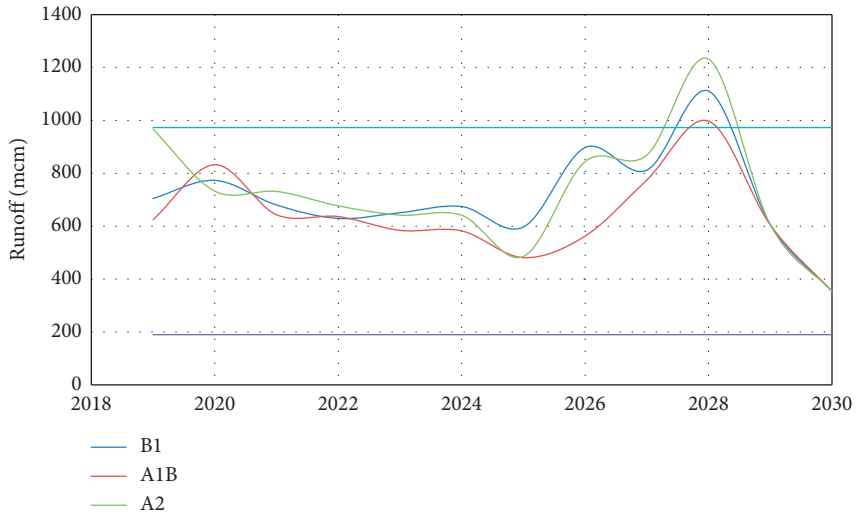


Figure 14: Comparison of the minimum and average observational runoff and the future near period under the ensemble model and the three emission scenarios.

three future periods under the ensemble model and the three emission scenarios.

In the above figures, R_OBS_MIN and R_OBS_AVE refer to the minimum and the average of a 28-year runoff input entering into the dam. As shown by the results, approximately in the entire durations of the three periods, a reduction occurred in the runoff input of the dam (Figures 14–16). This produced noticeable effects on the region's environment and water resources and needed a comprehensive planning for adjustment to the new conditions to tackle the resulting challenges.

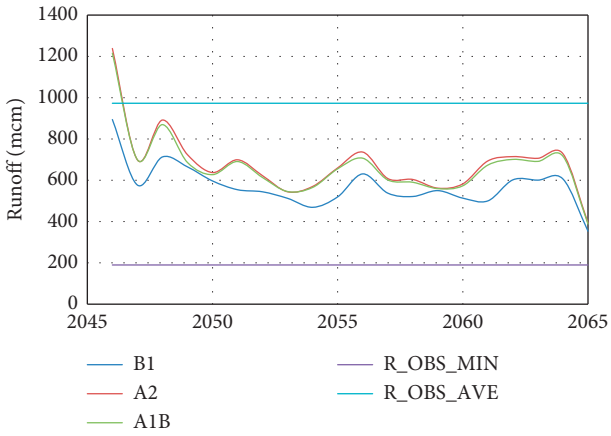


Figure 15: Comparison of the minimum and average observational runoff and the future middle period under the ensemble model and three emission scenarios.

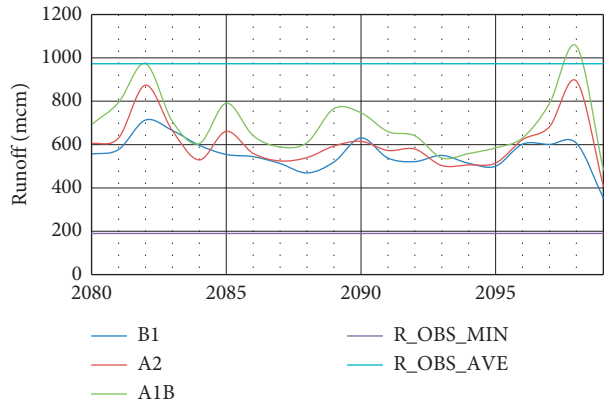


Figure 16: Comparison of the minimum and average observational runoff and the future far period under ensemble model and the three emission scenarios.

## 3. Conclusion

15 climatic models of CMIP3 series outputs available in LARS-WG database under three main greenhouse gas emission scenarios including B1, A2, and A1B were used to downscale and evaluate the climatic change effects on the meteorological and hydrological parameters in the Doroudzan dam catchment during three future periods. After the evaluation of the model precision for all stations, rainfall and temperature of the three future periods were simulated. Due to the various uncertainties of GCMs and emission scenarios, observational data, the distinctive resolution of any single model, the solution methods of governing equations, and boundary conditions and other sources of uncertainty, different outputs were obtained for the models. However, under most models and scenarios, an increase in the minimum and maximum daily temperatures and a decrease in the annual rainfall were observed. A shift was also observed in the annual pattern of rainfall (i.e., rainfall with a year). In other words, precipitation in the early months of the year was reduced while there was an increase in some of the other months. In this context, in order to mitigate the effects of this phenomenon on water resources and to avoid environmental problems such as decreased surface and underground water resources and the increased evaporation and perspiration and drying up of lakes and lagoons, and the formation of aerosol centers, it is required to do some long-term managerial planning to face and handle these challenges. In spite of the numerous models and the vast range of changes in the meteorological parameters in all the future periods, ensemble approach has chosen to reduce the uncertainties of outcomes of models for better planning. The scenario file of this ensemble model was produced by averaging the scenario files' parameters of 15 GCMs, and the meteorological parameters of the ensemble model under all three considered emission scenarios in all three future periods were simulated. The output of the ensemble model was used as the input for the creation of the rainfall-runoff model using the neural network. Based on the results, the GFF neural network with the CG learning algorithm and an architecture of 4-4-4-1 showed the best performance. After that, the runoffs of the three future periods under the suggested model and the three main emission scenarios were simulated. The results showed that the patterns of runoff changes inside and outside a year were in agreement with those of the rainfall changes, indicating its reduction with respect to the long-term annual observational average value.

## Data Availability

The data used to support the findings of this study are available from the corresponding author upon request.

## Conflicts of Interest

The authors declare that they have no conflicts of interest.

## References

[1] S. Solomon et al., "Climate change 2007-the physical science basis: Working group I contribution to the fourth assessment report of the IPCC," vol. 4, Cambridge University Press, Cambridge, UK, 2007.

[2] C. Change, "The physical science basis. Summary for policymakers. Contribution of working group I to the fourth assessment report of the intergovernmental panel on climate change. Jelektronnyj resurs," 2007, http://www.ipcc.ch.

[3] A. W. Wood, L. R. Leung, V. Sridhar, and D. P. Lettenmaier, "Hydrologic implications of dynamical and statistical approaches to downscaling climate model outputs," *Climatic change*, vol. 62, no. 1–3, pp. 189–216, 2004.

[4] C. B. Chisanga, E. Phiri, and V. R. N. Chinene, "Statistical downscaling of precipitation and temperature using long Ashton research station weather generator in Zambia: a case of mount makulu agriculture research station," *American Journal of Climate Change*, vol. 6, no. 3, pp. 487–512, 2017.

[5] R. Awal, H. Bayabil, and A. Fares, "Analysis of potential future climate and climate extremes in the Brazos Headwaters basin, Texas," *Water*, vol. 8, no. 12, p. 603, 2016.

[6] D. Kumar, D. S. Arya, A. R. Murumkar, and M. M. Rahman, "Impact of climate change on rainfall in Northwestern

Bangladesh using multi-GCM ensembles," *International Journal of Climatology*, vol. 34, no. 5, pp. 1395–1404, 2014.

[7] Z. Hao, Q. Ju, W. Jiang, and C. Zhu, "Characteristics and scenarios projection of climate change on the Tibetan plateau," *The Scientific World Journal*, vol. 2013, Article ID 129793, 9 pages, 2013.

[8] A. Salajegheh, A. Fathabadi, and M. Mahdavi, "Investigation on the efficiency of neuro-fuzzy method and statistical models in simulation of rainfall-runoff process," *Journal of Range and Watershed Management*, vol. 62, no. 1, pp. 65–79, 2009.

[9] J. Sinha, "A comparison of network types in artificial neural network-based rainfall-runoff modelling," *International Journal of Applied Research on Information Technology and Computing*, vol. 8, no. 1, pp. 41–50, 2017.

[10] A. B. Patel and G. S. Joshi, "Modeling of rainfall-runoff correlations using artificial neural network-A case study of Dharoi Watershed of a Sabarmati river basin, India," *Civil Engineering Journal*, vol. 3, no. 2, pp. 78–87, 2017.

[11] M. Zarghami, A. Abdi, I. Babaeian, Y. Hassanzadeh, and R. Kanani, "Impacts of climate change on runoffs in East Azerbaijan, Iran," *Global and Planetary Change*, vol. 78, no. 3-4, pp. 137–146, 2011.

[12] M. Bahri, M. Dastorati, and M. Goodarzi, "Investigation of droughts in 2011-2030 under climate change effects, a case study of Eskandari basin in Isfahan province, Iran," *Engineering and Management of Basins*, vol. 7, no. 2, pp. 157–171, 2015.

[13] H. I. J. Al-Safi and P. R. Sarukkalige, "Assessment of future climate change impacts on hydrological behavior of Richmond River Catchment," *Water Science and Engineering*, vol. 10, no. 3, pp. 197–208, 2017.

[14] M. H. Kashani, Y. Ghorbani, and S. Shahmorad, "Integration of Volterra model with artificial neural networks for rainfall-runoff simulation in forested catchment of northern Iran," *Journal of Hydrology*, vol. 540, pp. 340–354, 2016.

[15] Z. Li, G. Huang, X. Wang, J. Han, and Y. Fan, "Impacts of future climate change on river discharge based on hydrological inference: a case study of the Grand River Watershed in Ontario, Canada," *Science of The Total Environment*, vol. 548-549, pp. 198–210, 2016.

[16] Mislan, Haviluddin, S. Hardwinarto, Sumaryono, and M. Aipassa, "Rainfall monthly prediction based on artificial neural network: a case study in Tenggarong station, East Kalimantan-Indonesia," *Procedia Computer Science*, vol. 59, pp. 142–151, 2015.

[17] J. Farajzadeh, A. Fakheri Fard, and S. Lotfi, "Modeling of monthly rainfall and runoff of Urmia lake basin using "feed-forward neural network" and "time series analysis" model," *Water Resources and Industry*, vol. 7-8, pp. 38–48, 2014.

[18] S. Asadi, J. Shahrabi, P. Abbaszadeh, and S. Tabanmehr, "A new hybrid artificial neural networks for rainfall-runoff process modeling," *Neurocomputing*, vol. 121, pp. 470–480, 2013.

[19] K. Solaimani, "Rainfall-runoff prediction based on artificial neural network (a case study: Jarahi Watershed)," *American-Eurasian Journal of Agricultural and Environmental Sciences*, vol. 5, no. 6, pp. 856–865, 2009.

[20] C. Bishop and C. M. Bishop, *Neural Networks for Pattern Recognition*, Oxford University Press, Oxford, UK, 1995.

[21] M. Michie, "Introduction," in *Working Cross-Culturally*, pp. 1–12, Springer, Berlin, Germany, 2014.

[22] M. Semenov and P. Stratonovitch, "Use of multi-model ensembles from global climate models for assessment of climate change impacts," *Climate research*, vol. 41, no. 1, pp. 1–14, 2010.

[23] M. A. Semenov, E. M. Barrow, and A. Lars-Wg, *A Stochastic Weather Generator for Use in Climate Impact Studies*, User Man Herts UK, 2002.

[24] A. Comer, A. Fenech, and W. Gough, "Selecting a global climate model for understanding future scenarios of climate change," *Linking Climate Models To Policy And Decision-Making*, pp. 133–145, 2007, http://projects.upei.ca/climate/publications/linking-climate-models-to-policy-and-decision-making-2007/.

[25] J. Wang et al., "A novel conjugate gradient method with generalized Armijo search for efficient training of feedforward neural networks," *Neurocomputing*, vol. 275, pp. 308–316.

[26] J. Wang, W. Wu, and J. M. Zurada, "Deterministic convergence of conjugate gradient method for feedforward neural networks," *Neurocomputing*, vol. 74, no. 14-15, pp. 2368–2376, 2011.